INSTITUTE OF PHYSICS PUBLISHING JOURNAL OF MICROMECHANICS AND MICROENGINEERING

J. Micromech. Microeng. **15** (2005) 710–719 doi:10.1088/0960-1317/15/4/007

Microfluidic analysis of electrokinetic streaming potential induced by microflows of monovalent electrolyte solution

Myung-Suk Chun, Tae Seok Lee and Nak Won Choi[1]

Complex Fluids Research Lab, Korea Institute of Science and Technology (KIST), PO Box 131, Cheongryang, Seoul 130-650, Republic of Korea

E-mail: mschun@kist.re.kr

Received 1 October 2004, in final form 30 December 2004
Published 2 February 2005
Online at stacks.iop.org/JMM/15/710

Abstract

We develop a theoretical model of the electrokinetic streaming potential considering the Navier–Stokes equation coupled with the Poisson–Boltzmann equation in order to elaborate the possible applicability of the microfluidic-battery from conceptualization to system validation. The ion transport in the microchannel is described on the basis of the Nernst–Planck equation. In this study, monovalent symmetric electrolytes are considered, and the profile of fluid conductivity is derived in terms of both the concentration profile and the mobilities of anions and cations. The present simulations provide that the flow-induced streaming potential increases with increasing surface potential of microchannel wall, whereas increasing the surface conductivity reduces the streaming potential. We also present the results on the change of streaming potential with variations of the electric double layer thickness normalized by the channel radius. It is of interest to find the behavior that a lower value of ion mobility leads to the enhancement of streaming potential, which tends to develop with either increasing bulk electrolyte concentration or decreasing surface conductivity. Hence, a choice of electrolyte should be considered to obtain improved performance.

(Some figures in this article are in colour only in the electronic version)

Nomenclature

A	cross-sectional area of microchannel (m^2)
a	radius of microchannel (m)
E_z	flow-induced electric field in axial direction ($V\ m^{-1}$)
e	elementary charge (C)
F_z	body force in axial direction ($N\ m^{-3}$)
I	net electric current (A)
I_0, I_1	modified Bessel function of the first kind of zeroth and first order (–)
I_C	conduction current (A)
$I_{C,f}$	conduction current flowing through the bulk electrolyte solution (A)
$I_{C,s}$	conduction current flowing through the microchannel surface (A)
I_L	external current (A)
I_S	streaming current, or convection current (A)
K	mobility of ion species ($mol\ s\ kg^{-1}$)
k	Boltzmann constant ($J\ K^{-1}$)
L	length of microchannel (m)
N	number of microchannels (–)
N_A	Avogadro's number (mol^{-1})
n	number concentration of ion species (m^{-3})
p	hydraulic pressure (bar)
q	volumetric flow rate ($m^3\ s^{-1}$)
$\widetilde{R}$	total resistance of single microchannel (Ω)
R_f	fluid resistance (Ω)
R_L	external resistance (Ω)
R_s	surface resistance (Ω)

[1] Present address: School of Chemical and Biomolecular Engineering, Cornell University, Ithaca, NY 14853, USA.

r	radial distance in cylindrical coordinates (m)
t	time (s)
T	absolute temperature (K)
v	fluid velocity component (m s^{-1})
$\mathbf{v}_d$	drift velocity of ion species (m s^{-1})
Z	valence of ion species (–)
z	axial distance in cylindrical coordinates (m)

Greek symbols

ε	dielectric constant, or permittivity of the medium (C^2 J^{-1} m^{-1})
η	fluid viscosity (kg m^{-1} s^{-1})
κ	inverse EDL thickness (m^{-1})
λ_f	fluid conductivity (S m^{-1})
λ_s	specific surface conductivity (S)
ρ	fluid density (kg m^{-3})
ρ_e	net charge density (C m^{-3})
ϕ	flow-induced streaming potential (V)
ϕ_M	streaming potential for multi-channel array circuit (V)
Ψ	dimensionless electric potential (–)
Ψ_s	dimensionless electric surface potential (–)
ψ	electric potential (V)
ψ_s	electric surface potential (V)

Subscripts

b	bulk electrolyte
i	ion species
+	cation
−	anion

1. Introduction

A fundamental understanding of the electrokinetic phenomena is necessary in the design of diagnostic microdevices and micro-chips [1], microflow control in micro-electro mechanical system (MEMS) devices [2–4], and particle manipulation techniques [5]. Especially, electrokinetic techniques have the advantage of being easily integrable into microfluidic systems when compared to external systems [6]. Electrokinetic phenomena can be categorized into four types. Both electro-osmosis and electrophoresis use an applied electric field to induce motion, whereas both the streaming potential and the sedimentation potential have the opposite electrokinetic coupling in that they use motion to produce an electric field. Basically, such electrokinetic phenomena are present due to the electric double layer (EDL), which forms as a result of the distribution of electric charges near a dielectric charged surface [7, 8].

Lots of previous works in the area of electrokinetic transport phenomena mainly focus on electro-osmotic flow. It should also be recognized that the streaming potential has been an emergent technique for electrokinetic surface characterization of materials with solid–liquid interfaces. From the relations involving a quantitative expression of the force that creates the observed electrokinetic phenomena, the measurement of the streaming potential permits the determination of the zeta potential of the hydrodynamic phase boundary [9–13]. Examples include the electrokinetic characterization of an adsorption layer of fibrinogen on top of the fluoropolymer layer, performed using an electrokinetic microslit device [14].

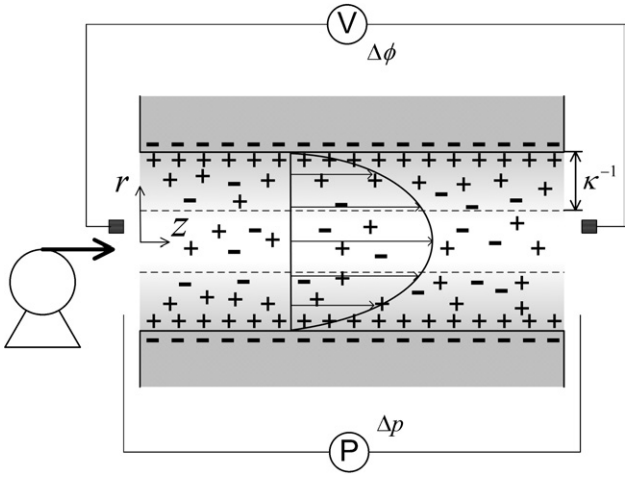

Figure 1. Schematic of electrokinetic streaming potential in a microfluidic channel.

Very recently, Yang *et al* [15] revealed a new fact that the streaming potential is applicable to an electrokinetic micro battery consisting of an array of microchannels. They conducted analytical solutions of the time-dependent microflow, and a good agreement was found between the predicted results and those from experiments for pressure-driven flow in microporous glass filter. Their results suggest that the hydrostatic pressure of a liquid can be converted into electrical work in the order of μW cm^{-3}, depending on the properties of the electrolyte solution and channel wall.

The phenomena concerning streaming potential as well as streaming current occur due to the charge displacement in the EDL caused by an external force shifting the liquid phase tangentially against the solid. As illustrated in figure 1, the counter-ions in the diffusive (or mobile) part of the EDL are carried toward the downstream end for the applied pressure p. Then the streaming current results in the pressure-driven flow direction of electrolyte solution, and the streaming potential ϕ generates corresponding to this streaming current. This flow-induced streaming potential acts to drive the counter-ions in the mobile part of the EDL to move in the direction opposite to the streaming current. This opposite-directional flow of ions will generate the conduction current in the Stern layer of the EDL. The overall result is a reduced flow rate in the direction of the pressure drop referred to as the electroviscous effect [16–18]. The convective transport of hydrodynamically mobile ions can be detected by measuring the streaming potential between the two electrodes positioned up- and downstream in the liquid flow, in which the internal resistance of the multi-meter used is sufficiently high.

With current MEMS and fabrication technologies, it is predicted that the streaming potential technique will become an established process in the field of electrokinetic microfluidics. In view of this aspect, we present an in depth analysis of the microfluidics in a microchannel encompassing electrokinetic phenomena. The equation of motion for an incompressible ionic fluid is developed by verifying the external body force and the relevant flow-induced electric field, from the

theoretical analysis of the Navier–Stokes (N–S) equation coupled with the Poisson–Boltzmann (P–B) equation. The basic principle of net current conservation is faithfully applied in the microchannel taking into account the Nernst–Planck (N–P) equation. For the case of higher surface potential, the finite difference method is employed in the nonlinear P–B equation. The flow-induced streaming potential is estimated with variations of the surface conductivity of the microchannel, bulk electrolyte concentration and the microchannel radius. We address a performance comparison of two kinds of 1:1 type electrolytes in order to indicate the importance of practical consideration of the individual ion mobilities in studying the electrokinetic streaming potential.

2. Theoretical analysis of electrokinetic microflow

Consider a model for pressure-driven and steady-state electrokinetic flow through a uniformly charged straight cylindrical microchannel. The development of the electrokinetic flow equation extends those of previous works [19, 20] to symmetric electrolytes in which the mobilities of anions and cations may individually be specified. Cylindrical coordinates (r, θ, z) are introduced, where r denotes the radial distance from the center axis and z is the distance along the axis of a microchannel.

2.1. Electric field in a charged cylindrical microchannel

When the charged surface is in contact with an electrolyte, the electrostatic charge would influence the distribution of nearby ions so that an electric field is established. In order to compute the electrokinetic streaming potential, the electric potential should first be evaluated. The positions of the individual ions in solution are replaced by the mean concentration of ions. It is well known that the nonlinear P–B equation governing the electric field is given as [7, 8]

$$\nabla^2\Psi = \kappa^2 \sinh\Psi. \tag{1}$$

Here, the dimensionless electric potential Ψ equals $Ze\psi/kT$ and the inverse EDL thickness (namely, inverse Debye radial thickness) κ is defined by

$$\kappa = \left(\frac{2n_{\mathrm{b}}Z_i^2e^2}{\varepsilon kT}\right)^{1/2}, \tag{2}$$

where n_{b} is the electrolyte ionic concentration in the bulk solution at the electroneutral state, Z_i is the valence of type-i ions, e is the elementary charge, ε is the dielectric constant and kT is the Boltzmann thermal energy. The Boltzmann distribution of the ionic concentration of type i (i.e., $n_i = n_{\mathrm{b}}\exp(-Z_ie\psi/kT)$) provides a local charge density Z_ien_i. Once the electric potential Ψ is obtained by applying the finite difference method provided in appendix A, it is straightforward to determine the net charge density $\rho_{\mathrm{e}}(\equiv \Sigma_i Z_ien_i = Ze(n_+ - n_-))$ as follows:

$$\rho_{\mathrm{e}} = Zen_{\mathrm{b}}[\exp(-\Psi) - \exp(\Psi)] = -2Zen_{\mathrm{b}}\sinh\Psi. \tag{3}$$

For a low potential of $\Psi \leqslant 1$ (i.e., less than $kT/e = 25.69$ mV) with a 1:1 type electrolyte system, the P–B equation may be linearized corresponding to the Debye–Hückel (D–H) approximation [7, 13]. For a cylindrical channel of radius a and length L, the linearized P–B equation leads to

$$\frac{1}{r}\frac{\mathrm{d}}{\mathrm{d}r}\left(r\frac{\mathrm{d}\Psi}{\mathrm{d}r}\right) = \kappa^2\Psi. \tag{4}$$

The boundary conditions are imposed as

$$\Psi = \Psi_{\mathrm{s}} \qquad \text{at} \quad r = a, \tag{5a}$$

$$\frac{\mathrm{d}\Psi}{\mathrm{d}r} = 0 \qquad \text{at} \quad r = 0. \tag{5b}$$

The solution to equation (4) can be obtained with these boundary conditions, and is derived as

$$\Psi(r) = \Psi_{\mathrm{s}}\frac{I_0(\kappa r)}{I_0(\kappa a)}, \tag{6}$$

where I_0 is the modified Bessel function of the first kind of zeroth order. From equations (4) and (6), the net charge density is then determined by

$$\rho_{\mathrm{e}} = -\varepsilon\nabla^2\psi = -\varepsilon\kappa^2\psi_{\mathrm{s}}\frac{I_0(\kappa r)}{I_0(\kappa a)}. \tag{7}$$

2.2. Flow field coupled with electrokinetic interaction

In principle, the N–S equation furnishes the paradigm for describing the equation of motion for an incompressible ionic fluid, given by

$$\rho\frac{\partial\mathbf{v}}{\partial t} + \rho(\mathbf{v}\cdot\nabla)\mathbf{v} = -\nabla p + \eta\nabla^2\mathbf{v} + \mathbf{F}, \tag{8}$$

where ρ and η are the density and viscosity of the fluid, respectively. Let us consider the one-dimensional laminar flow at the steady state through a cylindrical microchannel. The velocity, pressure and flow-induced electric field are expressed as $\mathbf{v} = [0, 0, v_z(r)]$, $p = p(z)$ and $\mathbf{E} = [0, 0, E_z(z)]$, respectively. Neglecting gravitational forces, the body force per unit volume $\mathbf{F}$ ubiquitously caused by the z-directional action of flow-induced electric field E_z on the net charge density ρ_{e} can be written as $F_z = \rho_{\mathrm{e}}E_z$ [16, 18]. With these identities, equation (8) reduces to

$$\eta\left[\frac{1}{r}\frac{\mathrm{d}}{\mathrm{d}r}\left(r\frac{\mathrm{d}v_z}{\mathrm{d}r}\right)\right] = \frac{\mathrm{d}p}{\mathrm{d}z} - \rho_{\mathrm{e}}E_z. \tag{9}$$

We would point out that the N–S equation corresponds to the Stokes equation for the flow situation of this study. E_z is defined by the flow-induced streaming potential ϕ as $E_z = -\mathrm{d}\phi(z)/\mathrm{d}z$, and the boundary conditions applied to $v_z(r)$ are

$$v_z(r) = 0 \qquad \text{at} \quad r = a, \tag{10a}$$

$$\frac{\mathrm{d}v_z(r)}{\mathrm{d}r} = 0 \qquad \text{at} \quad r = 0. \tag{10b}$$

In the case where the surface of the microchannel wall satisfies a condition of low potential ($\Psi_{\mathrm{s}} \leqslant 1$), equation (9) leads to the following expression:

$$\frac{1}{r}\frac{\mathrm{d}}{\mathrm{d}r}\left(r\frac{\mathrm{d}v_z}{\mathrm{d}r}\right) = \frac{1}{\eta}\left(\frac{\mathrm{d}p}{\mathrm{d}z}\right) - \frac{\varepsilon\kappa^2\psi_{\mathrm{s}}}{\eta}\frac{I_0(\kappa r)}{I_0(\kappa a)}\left(\frac{\mathrm{d}\phi}{\mathrm{d}z}\right). \tag{11}$$

Equation (11) can take an integral from 0 to L with respect to z together with setting $\Delta p = p_0 - p_{\mathrm{L}}$ and $\Delta\phi = \phi_0 - \phi_{\mathrm{L}}$. Then, the analytical solution for velocity profile $v_z(r)$ is derived as

$$v_z(r) = \frac{a^2 - r^2}{4\eta}\left(\frac{\Delta p}{L}\right) - \frac{\varepsilon\psi_{\mathrm{s}}}{\eta}\left[1 - \frac{I_0(\kappa r)}{I_0(\kappa a)}\right]\left(\frac{\Delta\phi}{L}\right). \tag{12}$$

In addition, the volumetric flow rate q gives

$$q = 2\pi \int_0^a v_z(r) r \, \mathrm{d}r = \frac{\pi a^4}{8\eta}\left(\frac{\Delta p}{L}\right) - \frac{\pi a^2 \varepsilon \psi_s}{\eta}\left[1 - \frac{2}{\kappa a}\frac{I_1(\kappa a)}{I_0(\kappa a)}\right]\left(\frac{\Delta \phi}{L}\right), \tag{13}$$

where I_1 is the modified Bessel function of the first kind of first order.

For a high surface potential ($\Psi_s > 1$), equation (11) can no longer be applied. By substituting equation (3) into equation (9), the N–S equation underlying the electrokinetic microflow is then expressed as

$$\frac{1}{r}\frac{\mathrm{d}}{\mathrm{d}r}\left(r\frac{\mathrm{d}v_z}{\mathrm{d}r}\right) = \frac{1}{\eta}\left(\frac{\mathrm{d}p}{\mathrm{d}z}\right) - \frac{2Zen_b}{\eta}\sinh\Psi\left(\frac{\mathrm{d}\phi}{\mathrm{d}z}\right). \tag{14}$$

We can derive a formula for the velocity profile subject to the above boundary conditions as

$$v_z(r) = \frac{a^2 - r^2}{4\eta}\left(\frac{\Delta p}{L}\right) - \frac{2Zen_b}{\eta}\left(\frac{\Delta \phi}{L}\right) \times \int_r^a \frac{1}{r}\left(\int_0^r r \sinh\Psi \, \mathrm{d}r\right)\mathrm{d}r. \tag{15}$$

In equation (15), the numerical integration is able to determine its solution. In a similar way, one obtains the volumetric flow rate by

$$q = \frac{\pi a^4}{8\eta}\left(\frac{\Delta p}{L}\right) - \frac{4\pi Zen_b}{\eta}\left(\frac{\Delta \phi}{L}\right) \times \int_0^a r\left[\int_r^a \frac{1}{r}\left(\int_0^r r \sinh\Psi \, \mathrm{d}r\right)\mathrm{d}r\right]\mathrm{d}r. \tag{16}$$

3. Electrokinetic flow-induced streaming potential

According to the N–P equation, the transport of ions in the channel is described in terms of convection and migration resulting from the pressure difference and electric potential gradient, respectively. The diffusion is not considered here by means of an assumption of no axial concentration gradient. Ions in the mobile region of the EDL are transported along with the solution flow through the channel length L, commonly causing the electric convection current (i.e., streaming current) I_S. The accumulation of ions sets up an electric field E_z with the streaming potential difference $\Delta\phi$ ($=E_z L$). This field causes the conduction current I_C to flow back in the opposite direction. At the steady state, the net current I should be zero as [10, 13, 14]

$$I \equiv I_S + I_C = 0. \tag{17}$$

3.1. Low potential problem

The streaming current is defined as an integration of the multiplication of the velocity profile and the net charge density, yielding

$$I_S = 2\pi \int_0^a \rho_e(r) v_z(r) r \, \mathrm{d}r. \tag{18}$$

For a low surface potential, equation (18) becomes

$$I_S = -\frac{\pi a^2 \varepsilon \psi_s}{\eta}\left[1 - \frac{2}{\kappa a}\frac{I_1(\kappa a)}{I_0(\kappa a)}\right]\left(\frac{\Delta p}{L}\right) - \frac{\pi a^2 \varepsilon^2 \kappa^2 \psi_s^2}{\eta} \times \left[1 - \frac{2}{\kappa a}\frac{I_1(\kappa a)}{I_0(\kappa a)} - \frac{I_1^2(\kappa a)}{I_0^2(\kappa a)}\right]\left(\frac{\Delta \phi}{L}\right). \tag{19}$$

Details of deriving equation (19) are provided in appendix B. The total resistance $\widetilde{R}$ along the microchannel consists of the surface resistance R_s and the fluid resistance R_f in parallel [15], so that

$$\widetilde{R} = \frac{1}{\left(\frac{1}{R_s} + \frac{1}{R_f}\right)} = \frac{R_s R_f}{R_s + R_f}. \tag{20}$$

Using Ohm's rule, the conduction current I_C can then be expressed as

$$I_C \equiv I_{C,s} + I_{C,f} = \frac{\Delta \phi}{\widetilde{R}}, \tag{21}$$

where $I_{C,s}$ ($=\Delta\phi/R_s$) is the conduction current through the microchannel wall and $I_{C,f}$ ($=\Delta\phi/R_f$) is the conduction current through the electrolyte solution. In equation (20), the surface resistance is readily defined as

$$R_s = L/2\pi a \lambda_s, \tag{22}$$

where $2\pi a$ equals the wetted perimeter and λ_s indicates the specific surface conductivity depending on the material property of microchannel.

Considering the contribution of radial concentration gradients to the electric current, the fluid resistance certainly varies with the radial position. It is reasonable that the influence of an axial concentration gradient upon the conduction current vanishes. For one-dimensional flow in a microchannel, the drift velocity of ion species i is given as

$$\mathbf{v}_{d,i} = -Z_i e N_A K_i \nabla \phi, \tag{23}$$

where N_A is the Avogadro's number and K_i is the mobility of ion species i defined as its velocity in the direction of an electric field of unit strength [9, 10]. Now the conduction current through the electrolyte solution for arbitrary channel cross-section can be expressed as follows:

$$I_{C,f} = \frac{\Delta \phi}{R_f} = \int_A \sum_i Z_i e n_i \mathbf{v}_{d,i} \, \mathrm{d}A = 2\pi Z^2 e^2 N_A \left(\frac{\Delta \phi}{L}\right)\int_0^a [K_+ n_+(r) + K_- n_-(r)] r \, \mathrm{d}r, \tag{24}$$

where the subscripts + and − of the ionic number concentration n_i denote the cations and the anions, respectively. From equation (24), we obtain the fluid resistance that is addressed as an inverse quantity of the integration of the local fluid conductivity λ_f over the cross-sectional area per axial channel length, expressed as

$$R_f = \frac{L}{2\pi \int_0^a \lambda_f(r) r \, \mathrm{d}r} = \frac{L}{2\pi Z^2 e^2 N_A \int_0^a [K_+ n_+(r) + K_- n_-(r)] r \, \mathrm{d}r}. \tag{25}$$

The total resistance can be identified as

$$\widetilde{R} = \frac{L}{2\pi\left[a\lambda_s + Z^2 e^2 N_A \int_0^a (K_+ n_+ + K_- n_-) r \, \mathrm{d}r\right]}. \tag{26}$$

Substituting equations (19) and (21) into equation (17) gives an analytic formula of the streaming potential for a low surface potential, namely

$$\Delta\phi = \frac{\frac{\pi a^2 \varepsilon \psi_s}{\eta}\left[1 - \frac{2}{\kappa a}\frac{I_1(\kappa a)}{I_0(\kappa a)}\right]\Delta p}{\frac{L}{\widetilde{K}} - \frac{\pi a^2 \varepsilon^2 \kappa^2 \psi_s^2}{\eta}\left[1 - \frac{2}{\kappa a}\frac{I_1(\kappa a)}{I_0(\kappa a)} - \frac{I_1^2(\kappa a)}{I_0^2(\kappa a)}\right]}. \tag{27}$$

If N microchannels are assembled in parallel and the external resistance is applied, then the net current is taken to be $I \equiv N(I_S + I_C) + I_L = 0$, where I_L means the external current. In a similar way, the streaming potential for a multi-channel array circuit can be obtained:

$$\Delta\phi_M = \frac{\frac{\pi a^2 \varepsilon \psi_s}{\eta}\left[1 - \frac{2}{\kappa a}\frac{I_1(\kappa a)}{I_0(\kappa a)}\right]\Delta p}{\frac{L}{\widetilde{K}} + \frac{L}{NR_L} - \frac{\pi a^2 \varepsilon^2 \kappa^2 \psi_s^2}{\eta}\left[1 - \frac{2}{\kappa a}\frac{I_1(\kappa a)}{I_0(\kappa a)} - \frac{I_1^2(\kappa a)}{I_0^2(\kappa a)}\right]} \tag{28}$$

and the external current passing the external resistance R_L is $I_L = \Delta\phi_M / R_L$.

3.2. High potential problem

The streaming current for a high surface potential is derived from equations (3), (15) and (18), as follows:

$$I_S = -\frac{\pi Z e n_b}{\eta}\left(\frac{\Delta p}{L}\right)\int_0^a r(a^2 - r^2)\sinh\Psi\,\mathrm{d}r + \frac{8\pi(Zen_b)^2}{\eta} \times \left(\frac{\Delta\phi}{L}\right)\int_0^a r\sinh\Psi\left[\int_r^a \frac{1}{r}\left(\int_0^r r\sinh\Psi\,\mathrm{d}r\right)\mathrm{d}r\right]\mathrm{d}r. \tag{29}$$

We combine the conduction current I_C defined as in equation (21), and then the streaming potential is finally written as the following expression:

$$\Delta\phi = \frac{\frac{\pi Z e n_b}{\eta}\left[\int_0^a r(a^2 - r^2)\sinh\Psi\,\mathrm{d}r\right]\Delta p}{\frac{L}{\widetilde{K}} + \frac{8\pi(Zen_b)^2}{\eta}\int_0^a r\sinh\Psi\left[\int_r^a \frac{1}{r}\left(\int_0^r r\sinh\Psi\,\mathrm{d}r\right)\mathrm{d}r\right]\mathrm{d}r}. \tag{30}$$

In equation (30), the electric potential profile is determined by using the finite difference method. In order to satisfy the accuracy requirement, our numerical simulations were run with grids of 5×10^3 built within the channel and the convergence criterion is given as 10^{-8}. By the corresponding analogy, we again derive the streaming potential for a multi-channel array circuit, expressed as

$$\Delta\phi_M = \frac{\frac{\pi Z e n_b}{\eta}\left[\int_0^a r(a^2 - r^2)\sinh\Psi\,\mathrm{d}r\right]\Delta p}{\frac{L}{\widetilde{K}} + \frac{L}{NR_L} + \frac{8\pi(Zen_b)^2}{\eta}\int_0^a r\sinh\Psi\left[\int_r^a \frac{1}{r}\left(\int_0^r r\sinh\Psi\,\mathrm{d}r\right)\mathrm{d}r\right]\mathrm{d}r} \tag{31}$$

from which one can determine the external current $I_L = \Delta\phi_M / R_L$.

4. Results and discussion

Illustrative computations are performed considering a fully developed laminar flow of the aqueous solution of a monovalent electrolyte. We assume a cylindrical microchannel made of inorganic materials such as glass or fused silica. At room temperature, the dielectric constant and the viscosity of the fluid are taken as $\varepsilon = 80 \times (8.854 \times 10^{-12})\,\mathrm{C^2\,J^{-1}\,m^{-1}}$ and $\eta = 1.0 \times 10^{-3}\,\mathrm{kg\,m^{-1}\,s^{-1}}$, respectively. The ionic concentration of the 1:1 type electrolyte equals the ionic strength of the solution, in which the EDL thickness κ^{-1} (nm) subject to equation (2) is given by (solution ionic strength (mol))$^{-1/2}$/3.278. The EDL thicknesses with variations of bulk electrolyte concentrations is provided in table 1.

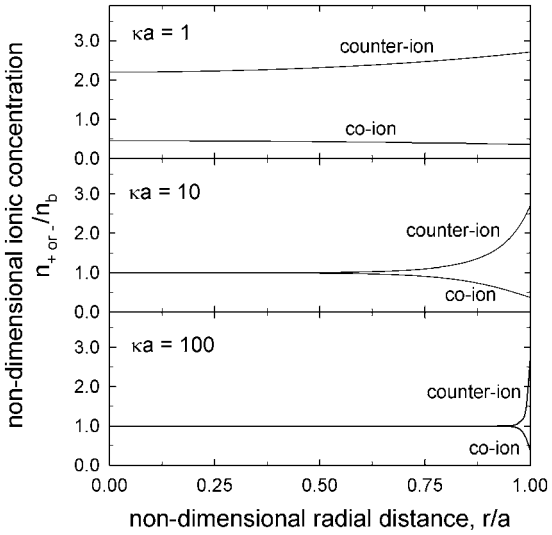

Figure 2. Number density profiles for co- and counter-ions in a microchannel for several dimensionless inverse EDL thicknesses, $\Psi_s = 1$.

Table 1. The condition of 1:1 type electrolyte aqueous solution.

[a]Bulk electrolyte concentration C_b (mM)	EDL thickness κ^{-1} (nm)
10^{-3}	305
10^{-2}	96.5
10^{-1}	30.5
1.0	9.7
10	3.1

[a] $n_b\,(1/\mathrm{m^3}) = N_A \times C_b$.

Figure 2 shows the dimensionless number concentrations of co- and counter-ions along the radial distance for several dimensionless inverse EDL thicknesses κa. The counter-ion of electrolyte is oppositely charged against the surface of microchannel wall. Thinning of the EDL means the decrease of electrostatic interaction. An increase in κa from 1 to 10 results from changes of either a ten times increase in the microchannel radius for the constant bulk electrolyte concentration or a hundred times increase in the bulk concentration for the constant radius. A κa value of 1 means that the EDL thickness κ^{-1} is equal to the microchannel radius a. When the EDL thickness exceeds the microchannel radius, the overlap of the EDL inside the microchannel results in a radial concentration gradient. It has been known that the concentration gradient arising in the case of κa less than 1 really affects the generation of the flow-induced streaming potential [21]. In accordance with the Boltzmann distribution and the D–H approximation, dimensionless number concentrations of each ion at the wall

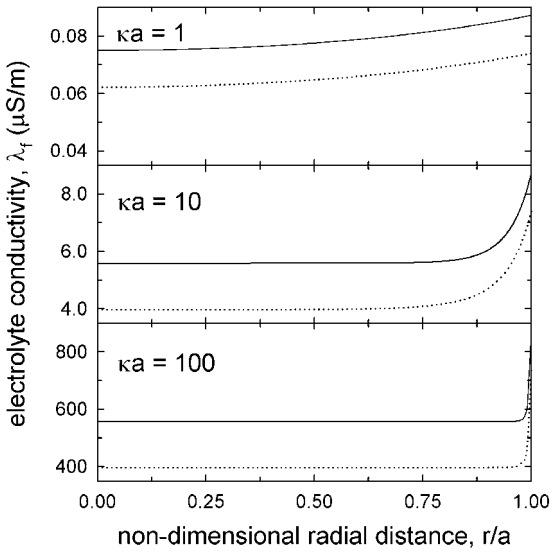

Figure 3. Fluid conductivity profiles for several dimensionless inverse EDL thicknesses for monovalent electrolytes of KCl (full) and $LiClO_4$ (dotted), $\Psi_s = 1$.

Table 2. Mobilities of ions in aqueous solutions at 298.15 K.

Monovalent electrolyte	Ions (cation, anion)	Mobility (10^{-13} mol s kg^{-1})
KCl	K^+	7.91
(potassium chloride)	Cl^-	8.19
$LiClO_4$	Li^+	4.16
(lithium perchlorate)	ClO_4^-	7.29

are

$$n_{\text{co-ion}}/n_b = e^{-1} \cong 0.37, \tag{32a}$$

$$n_{\text{counter-ion}}/n_b = e^{+1} \cong 2.72. \tag{32b}$$

As the 1:1 type electrolytes, both KCl and $LiClO_4$ are considered. Their individual ion mobilities provided in table 2 can be estimated from molar conductances of infinite dilution based on the Kohlrausch rule of the migration of ions [22]. Li^+ has the lowest mobility, indicating that the resistance to its motion through the solution is highest. Figure 3 shows the profile of fluid conductivity, i.e., $\lambda_f(r) = Z^2e^2N_A[K_+n_+(r) + K_-n_-(r)]$. The position where the fluid conductivity λ_f reaches the bulk value moves towards the channel wall as κa increases. The overall profile of fluid conductivity of KCl exhibits an enhancement compared to that of $LiClO_4$. As in figure 2, the fluid conductivity for extremely weak screening of $\kappa a = 1$ does not reach its bulk value even at the center region of the channel. For $\kappa a = 10$, the bulk fluid conductivities are 5.58 μS m^{-1} for KCl and 3.97 μS m^{-1} for $LiClO_4$, which relatively correspond to the literature value. Figures 2 and 3 allow us to understand the significance of both the microchannel radius and the bulk electrolyte concentration as design parameters regarding an efficient tool for energy conversion, under the name of electrokinetic microfluidic-battery in this study.

Figures 4(a) and (b) demonstrate how the streaming potential changes with variations of the surface conductivity

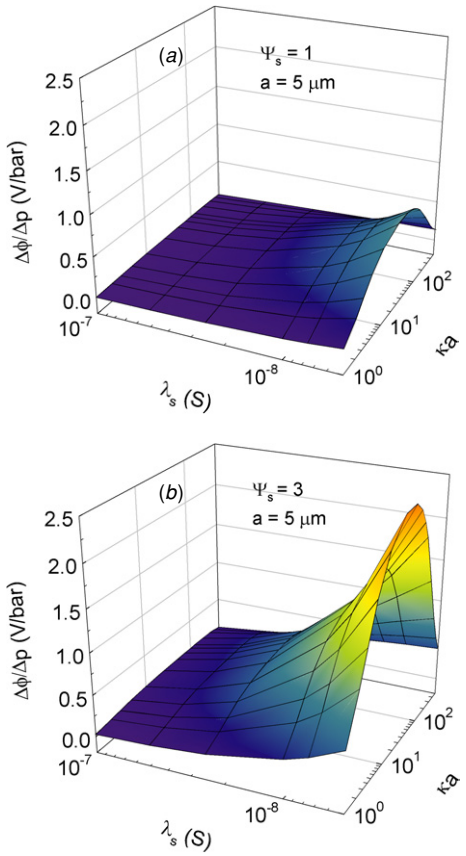

Figure 4. Effect of bulk concentration of KCl electrolyte on $\Delta\phi/\Delta p$ with different surface conductivities λ_s for (a) $\Psi_s = 1$ and (b) $\Psi_s = 3$, where $\Delta p = 10$ bar and $L = 10^{-2}$ m.

λ_s as well as the bulk electrolyte concentration for the constant microchannel radius of 5 μm. Plotting the streaming potential coefficient ($=\Delta\phi/\Delta p$) it can be verified that simulation results are related to the performance evaluation. The optimum flow rate should be considered to keep up with the pressure drop. The bulk fluid conductivity of the monovalent symmetric electrolyte is almost much greater than the surface conductivity of the channel made of inorganic or polymeric materials [7, 13]. For example, the glass made of borosilicate material has a surface conductivity of about 10^{-2} μS [11, 14]. The increasing trend in $\Delta\phi/\Delta p$ with decreasing surface conductivity is more considerable for higher surface potential as shown in figure 4(b). If Δp of 1 bar is applied, the value of streaming potential increases to about 2.5 V, although that is a theoretical prediction.

We note that there exists a maximum value of $\Delta\phi/\Delta p$ in figures 4(a) and (b). In the low-κa region, the rate of increase in the streaming current is much higher than that of the total resistance $\widetilde{R}$. In fact, the total resistance remains almost constant compared with the streaming current I_S, appearing as a rise of $\Delta\phi/\Delta p$ with increasing bulk electrolyte concentration. The amount of mobile ions becomes saturated after a rapid increase in the streaming current; therefore, the streaming current approaches the plateau regime around a maximum point. As the bulk electrolyte concentration continues to increase, the total resistance decreases, whereas the streaming current remains constant.

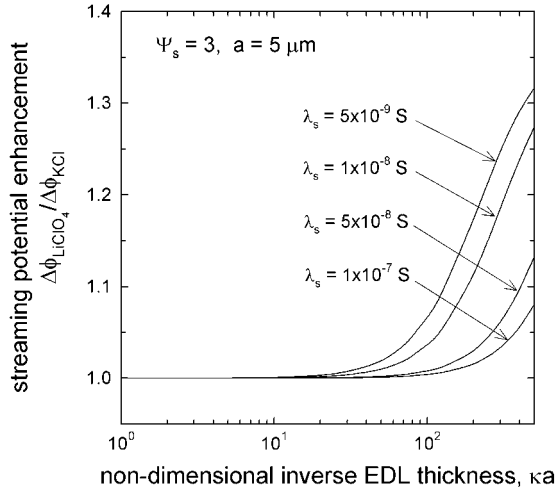

Figure 5. Effect of bulk electrolyte concentration on $\Delta\phi_{LiClO_4}/\Delta\phi_{KCl}$ with different surface conductivities λ_s, where $\Delta p = 10$ bar and $L = 10^{-2}$ m.

In practice, higher streaming potential is obtained in $LiClO_4$ electrolyte due to lower mobilities of ions as given in table 2. This behavior can obviously be seen in figure 5. The enhancement of the streaming potential in $LiClO_4$ electrolyte is more developed with either increasing bulk electrolyte concentration or decreasing surface conductivity.

In figures 6(*a*) and (*b*), the streaming potential is computed with variations of the surface conductivity as well as the microchannel radius for a constant bulk electrolyte concentration of 0.1 mM KCl. The streaming potential rises entirely with increasing radius; however, a gentle slope is shown eventually for larger κa. This increasing behavior can be explained by two factors: one is the convective effect of the streaming current implicating the numerator of equations (27) and (30), and the other comes from the total resistance. The total resistance remains almost constant at the constant bulk electrolyte concentration, whereas the convective effect of the streaming current increases with increasing radius, guaranteeing the increase of $\Delta\phi/\Delta p$.

As demonstrated in figures 4 and 6, the flow-induced streaming potential increases with decreasing surface conductivity of the microchannel. Once the surface conductivity becomes lower, a deficiency of the conduction current occurs. Based on the principle of net current conservation, higher streaming potential should necessarily be generated to make up the deficiency. In figure 7, the enhancement of the streaming potential in $LiClO_4$ electrolyte is quantified again, which is developed with increasing radius. The adoption of electrolyte with lower mobility is shown to result in improved performance; therefore, a proper choice of electrolyte solution plays an important role in the microfluidic-battery.

The power density can be evaluated from the power ($=\phi_M I_L$) divided by the overall volume of microchannels for the imposed external resistance. As an example, we present figure 8 for the case of $LiClO_4$ electrolyte, where a higher pressure difference increases the power density, as expected. It also increases with increasing either the number of channels or the external resistance. Figure 8 illustrates that, depending on the electrokinetic properties, our theoretical prediction results

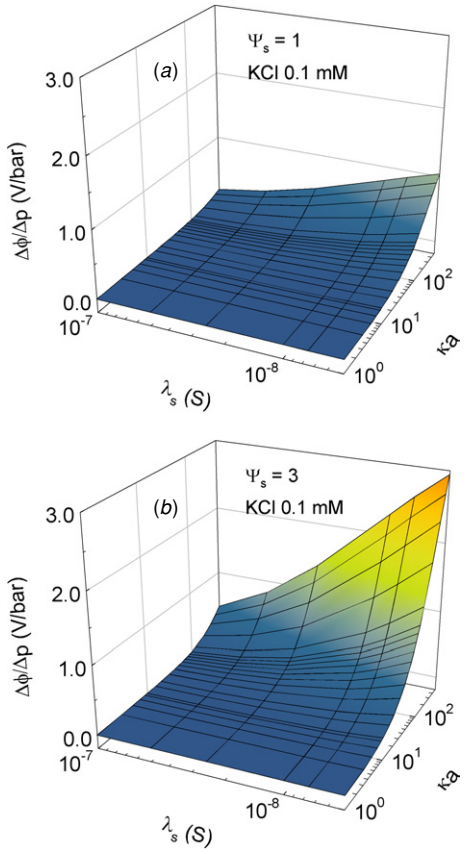

Figure 6. Effect of microchannel radius a on $\Delta\phi/\Delta p$ with different surface conductivities λ_s for (*a*) $\Psi_s = 1$ and (*b*) $\Psi_s = 3$, where $\Delta p = 10$ bar and $L = 10^{-2}$ m.

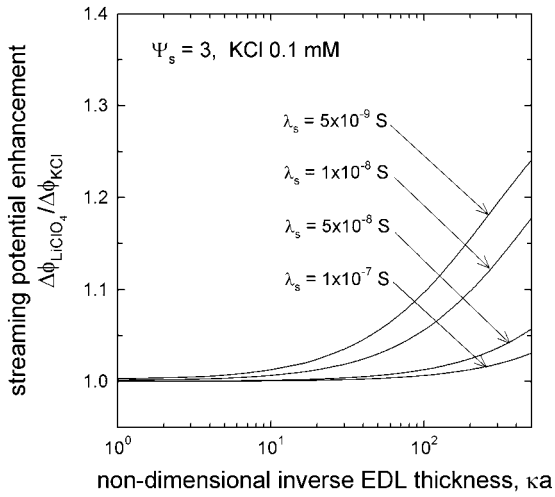

Figure 7. Effect of microchannel radius a on $\Delta\phi_{LiClO_4}/\Delta\phi_{KCl}$ with different surface conductivities λ_s, where $\Delta p = 10$ bar and $L = 10^{-2}$ m.

in the higher order of magnitude for the power densities reported in the literature [15, 23]. For a large N, one can observe that the power density takes values above 1 μW cm^{-3} even at a low Δp (i.e., less than 1 bar).

Further studies are required to access the present analysis of the practical system. Instead of the glass filter used in the previous work [15], we suggest more useful microdevices

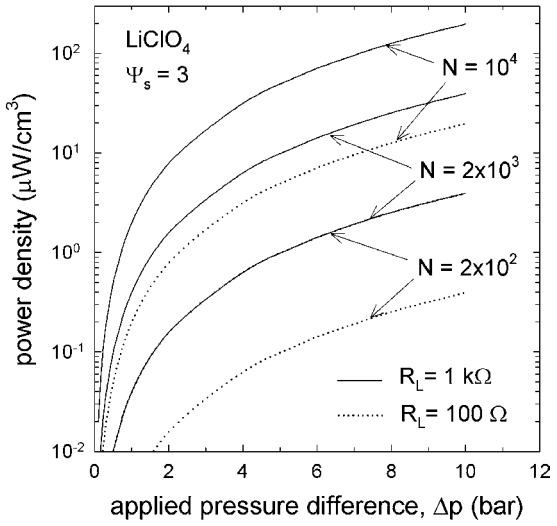

Figure 8. The predicted power density for $LiClO_4$ electrolyte as a function of Δp with different external resistances and numbers of channels, where $a = 5\ \mu$m, $\kappa a = 10$, $L = 2 \times 10^{-3}$ m and $\lambda_s = 5 \times 10^{-9}$ S.

such as microfluidic-chip with multi-channel type. In this context, it may open a new area of applied research in MEMS technology.

5. Conclusions

This study generates interest in and motivates research on emerging MEMS technologies and micromachining techniques, which have been increasingly employed in the electrokinetic microfluidic system. We developed a theoretical model concerning the streaming potential from analyzing the electrokinetic microflow in a cylindrical microchannel, and simulated the N–S equation coupled with the P–B equation.

The profile of fluid conductivity incorporated with the concentration profile of both co- and counter-ions has been estimated for two kinds of inorganic electrolytes, i.e., KCl and $LiClO_4$. To get the design methodology in the electrokinetic microfluidic-battery, one should consider the basic parameter variations of the surface potential of a microchannel wall, the surface conductivity λ_s, the microchannel radius a, the electrolyte concentration of bulk solution and the pressure drop across microchannel Δp. These variations emphasize the physical implementation and the system performance.

The flow-induced streaming potential certainly increases with increasing surface potential of the microchannel wall. Decreasing the surface conductivity leads to a higher streaming potential, due to the making up mechanism for the deficiency of conduction current in connection with the principle of net current conservation. Simulation results show that the streaming potential increases with increasing microchannel radius. Interestingly, a maximum value of the streaming potential could be obtained with variations of bulk electrolyte concentration when the microchannel radius is constant. It has been observed that the enhancement of streaming potential encountered in the electrolyte with lower ion mobility is developed with either increasing bulk concentration or decreasing surface conductivity.

Acknowledgments

This work was supported by the Basic Research Fund (R01-2001-000-00411-0) from the KOSEF as well as the International Collaboration Research Fund (M6-0302-00-0005) from the Korea Ministry of Science and Technology.

Appendix A. Electric potential by finite difference scheme

To obtain the solution of the nonlinear P–B equation with the boundary conditions, taking the five-point central difference method yields the left-hand side of equation (1) as

$$\frac{d\Psi}{dr} = \frac{\Psi_{j+1}^{k+1} - \Psi_{j-1}^{k+1}}{2\Delta r} \tag{A1}$$

$$\frac{d^2\Psi}{dr^2} = \frac{\Psi_{j+1}^{k+1} - 2\Psi_{j}^{k+1} + \Psi_{j-1}^{k+1}}{\Delta r^2}, \tag{A2}$$

where k is the iteration index and the grid index $j = 1, 2, \ldots, N$. The functions on the right-hand side of equation (1) can be linearized as [18]

$$\sinh\Psi = \sinh\Psi_j^k + \left(\Psi_j^{k+1} - \Psi_j^k\right)\cosh\Psi_j^k. \tag{A3}$$

From equations (A1), (A2) and (A3), the finite difference form of the nonlinear P–B equation becomes

$$\frac{\Psi_{j+1}^{k+1} - 2\Psi_{j}^{k+1} + \Psi_{j-1}^{k+1}}{\Delta r^2} + \frac{\Psi_{j+1}^{k+1} - \Psi_{j-1}^{k+1}}{2r_j\Delta r} = \kappa^2\left[\sinh\Psi_j^k + \left(\Psi_j^{k+1} - \Psi_j^k\right)\cosh\Psi_j^k\right]. \tag{A4}$$

Then, equation (A4) is rewritten as

$$(2r_j + \Delta r)\Psi_{j+1}^{k+1} - \left[4r_j + 2r_j(\kappa\Delta r)^2\cosh\Psi_j^k\right]\Psi_j^{k+1} + (2r_j - \Delta r)\Psi_{j-1}^{k+1} = 2r_j(\kappa\Delta r)^2\left(\sinh\Psi_j^k - \Psi_j^k\cosh\Psi_j^k\right). \tag{A5}$$

Equation (A5) can be solved for Ψ_j^{k+1} by successive iterative calculation, using the value of Ψ obtained in the kth iteration. The boundary condition at the wall (i.e., $\Psi|_{r=a} = \Psi_s$) gives

$$\Psi_N^{k+1} = \Psi_s, \tag{A6}$$

and at the center (i.e., $d\Psi/dr|_{r=0} = 0$)

$$\frac{\Psi_1^{k+1} - \Psi_{-1}^{k+1}}{2\Delta r} = 0. \tag{A7}$$

From a relation of $\Psi_{-1}^{k+1} = \Psi_1^{k+1}$ encountered in equation (A7), equation (A5) yields

$$2\Psi_1^{k+1} - \left[2 + (\kappa\Delta r)^2\cosh\Psi_0^k\right]\Psi_0^{k+1} = (\kappa\Delta r)^2\left(\sinh\Psi_0^k - \Psi_0^k\cosh\Psi_0^k\right). \tag{A8}$$

A series of algebraic equations can be expressed in a matrix form (i.e., $\mathbf{A\Psi} = \mathbf{b}$) given by

$$\begin{bmatrix}
P_0 & 2 & 0 & & \cdot & \cdot & \cdot & & 0 \\
f_{1,-} & P_1 & f_{1,+} & 0 & & & & & \\
 & \ddots & \ddots & \ddots & & & & & \cdot \\
 & 0 & f_{j-1,-} & P_{j-1} & f_{j+1,+} & 0 & & & \cdot \\
\cdot & & 0 & f_{j,-} & P_j & f_{j,+} & 0 & & \cdot \\
\cdot & & & 0 & f_{j+1,-} & P_{j+1} & f_{j+1,+} & 0 & \\
\cdot & & & & & \ddots & \ddots & \ddots & \\
 & & & & & 0 & f_{N-1,-} & P_{N-1} & f_{N-1,+} \\
0 & & \cdot & \cdot & \cdot & & & 0 & 1
\end{bmatrix}$$

$$\times \begin{bmatrix} \Psi_0^{k+1} \\ \Psi_1^{k+1} \\ \vdots \\ \Psi_{j-1}^{k+1} \\ \Psi_j^{k+1} \\ \Psi_{j+1}^{k+1} \\ \vdots \\ \Psi_{N-1}^{k+1} \\ \Psi_N^{k+1} \end{bmatrix} = \begin{bmatrix} Q_0 \\ Q_1 \\ \vdots \\ Q_{j-1} \\ Q_j \\ Q_{j+1} \\ \vdots \\ Q_{N-1} \\ \Psi_s \end{bmatrix}. \tag{A9}$$

In equation (A9), the constant potential boundary condition permits the following form:

$$f_{j,-} = 2r_j - \Delta r \tag{A10}$$

$$f_{j,+} = 2r_j + \Delta r \tag{A11}$$

$$P_j = -4r_j - 2r_j(\kappa\Delta r)^2 \cosh\Psi_j^k \tag{A12}$$

$$Q_j = 2r_j(\kappa\Delta r)^2\left(\sinh\Psi_j^k - \Psi_j^k\cosh\Psi_j^k\right), \tag{A13}$$

where $P_0 = -2 - (\kappa\Delta r)^2\cosh\Psi_0^k$ and $Q_0 = (\kappa\Delta r)^2\left(\sinh\Psi_0^k - \Psi_0^k\cosh\Psi_0^k\right)$.

Appendix B. Analytical solution for low potential problem

The relevant equation for the streaming current given in equation (19) is derived by substituting equations (7) and (12) into equation (18), and hence can be written as

$$I_S = -2\pi\int_0^a \varepsilon\kappa^2\psi_s\frac{I_0(\kappa r)}{I_0(\kappa a)}\left\{\left(\frac{a^2-r^2}{4\eta}\right)\left(\frac{\Delta p}{L}\right) - \frac{\varepsilon\psi_s}{\eta}\left[1-\frac{I_0(\kappa r)}{I_0(\kappa a)}\right]\left(\frac{\Delta\phi}{L}\right)\right\} r\,\mathrm{d}r. \tag{B1}$$

It is rearranged as

$$I_S = -\frac{\pi\varepsilon\kappa^2\psi_s}{2\eta}\left(\frac{\Delta p}{L}\right)\int_0^a (a^2-r^2)\frac{I_0(\kappa r)}{I_0(\kappa a)} r\,\mathrm{d}r + \frac{2\pi\varepsilon^2\kappa^2\psi_s^2}{\eta}\left(\frac{\Delta\phi}{L}\right)\int_0^a \frac{I_0(\kappa r)}{I_0(\kappa a)}\left[1-\frac{I_0(\kappa r)}{I_0(\kappa a)}\right] r\,\mathrm{d}r. \tag{B2}$$

Each term on the right-hand side of equation (B2) is identified as

$$I_{S,1} \equiv -\frac{\pi\varepsilon\kappa^2\psi_s}{2\eta}\left(\frac{\Delta p}{L}\right)\int_0^a (a^2-r^2)\frac{I_0(\kappa r)}{I_0(\kappa a)} r\,\mathrm{d}r = -\frac{\pi\varepsilon\kappa^2\psi_s}{2\eta I_0(\kappa a)}\left(\frac{\Delta p}{L}\right)\left[a^2\int_0^a r I_0(\kappa r)\,\mathrm{d}r - \int_0^a r^3 I_0(\kappa r)\,\mathrm{d}r\right], \tag{B3}$$

and

$$I_{S,2} \equiv \frac{2\pi\varepsilon^2\kappa^2\psi_s^2}{\eta}\left(\frac{\Delta\phi}{L}\right)\int_0^a \frac{I_0(\kappa r)}{I_0(\kappa a)}\left[1-\frac{I_0(\kappa r)}{I_0(\kappa a)}\right] r\,\mathrm{d}r = \frac{2\pi\varepsilon^2\kappa^2\psi_s^2}{\eta I_0(\kappa a)}\left(\frac{\Delta\phi}{L}\right)\left[\int_0^a r I_0(\kappa r)\,\mathrm{d}r - \frac{1}{I_0(\kappa a)}\int_0^a r I_0^2(\kappa r)\,\mathrm{d}r\right]. \tag{B4}$$

The integration by parts can be performed using the following:

$$\int_0^a r I_0(\kappa r)\,\mathrm{d}r = \frac{a}{\kappa}I_1(\kappa a) \tag{B5}$$

$$\int_0^a r^3 I_0(\kappa r)\,\mathrm{d}r = \frac{a^3}{\kappa}I_1(\kappa a) - \frac{2a^2}{\kappa^2}I_0(\kappa a) + \frac{4a}{\kappa^3}I_1(\kappa a) \tag{B6}$$

$$\int_0^a r I_0^2(\kappa r)\,\mathrm{d}r = \frac{a^2}{2}\left[I_0^2(\kappa a) - I_1^2(\kappa a)\right]. \tag{B7}$$

Substituting equations (B5) and (B6) into equation (B3) gives

$$I_{S,1} = -\frac{\pi a^2\varepsilon\psi_s}{\eta}\left(\frac{\Delta p}{L}\right)\left[1-\frac{2}{\kappa a}\frac{I_1(\kappa a)}{I_0(\kappa a)}\right], \tag{B8}$$

and substituting equations (B5) and (B7) into equation (B4) gives

$$I_{S,2} = -\frac{\pi a^2\varepsilon^2\kappa^2\psi_s^2}{\eta}\left(\frac{\Delta\phi}{L}\right)\left[1-\frac{2}{\kappa a}\frac{I_1(\kappa a)}{I_0(\kappa a)} - \frac{I_1^2(\kappa a)}{I_0^2(\kappa a)}\right]. \tag{B9}$$

Then, the streaming current can be obtained as

$$I_S = -\frac{\pi a^2\varepsilon\psi_s}{\eta}\left[1-\frac{2}{\kappa a}\frac{I_1(\kappa a)}{I_0(\kappa a)}\right]\left(\frac{\Delta p}{L}\right) - \frac{\pi a^2\varepsilon^2\kappa^2\psi_s^2}{\eta}\left[1-\frac{2}{\kappa a}\frac{I_1(\kappa a)}{I_0(\kappa a)} - \frac{I_1^2(\kappa a)}{I_0^2(\kappa a)}\right]\left(\frac{\Delta\phi}{L}\right). \tag{B10}$$

References

[1] Harrison J D, Fluri K, Seiler K, Fan Z H, Effenhauser C S and Manz A 1993 Micromachining a miniaturized capillary electrophoresis-based chemical analysis system on a chip *Science* **261** 895–7

[2] Polson N A and Hayes M A 2000 Electroosmotic flow control of fluids on a capillary electrophoresis microdevice using an applied external voltage *Anal. Chem.* **72** 1088–92

[3] Yang J and Kwok D Y 2003 Analytical treatment of flow in infinitely extended circular microchannels and the effect of slippage to increase flow efficiency *J. Micromech. Microeng.* **13** 115–23

[4] Chang C C and Yang R J 2004 Computational analysis of electrokinetically driven flow mixing in microchannels with patterned blocks *J. Micromech. Microeng.* **14** 550–8

[5] Effenhauser C S, Bruin G J, Paulus A and Ehrat M 1997 Integrated capillary electrophoresis on flexible silicone microdevices: analysis of DNA restriction fragments and detection of single DNA molecules on microchips *Anal. Chem.* **69** 3451–7

[6] Karniadakis G E and Beskok A 2003 *Micro Flows: Fundamentals and Simulation* (New York: Springer)

[7] Hunter R 1981 *Zeta Potential in Colloid Science: Principles and Applications* (London: Academic)

[8] Probstein R F 1994 *Physicochemical Hydrodynamics* (New York: Wiley)

[9] Bowen W R and Jenner F 1995 Electroviscous effects in charged capillaries *J. Colloid Interface Sci.* **173** 388–95

[10] Szymczyk A, Aoubiza B, Fievet P and Pagetti J 1999 Electrokinetic phenomena in homogeneous cylindrical pores *J. Colloid Interface Sci.* **216** 285–96

[11] Ren L, Li D and Qu W 2001 Electro-viscous effects on liquid flow in microchannels *J. Colloid Interface Sci.* **233** 12–22
[12] Sung J H, Chun M-S and Choi H J 2003 On the behavior of electrokinetic streaming potential during protein filtration with fully and partially retentive nanopores *J. Colloid Interface Sci.* **264** 195–202
[13] Chun M-S, Lee S-Y and Yang S-M 2003 Estimation of zeta potential by electrokinetic analysis of ionic fluid flows through a divergent microchannel *J. Colloid Interface Sci.* **266** 120–6
[14] Werner C, Körber H, Zimmermann R, Dukhin S and Jacobasch H-J 1998 Extended electrokinetic characterization of flat solid surfaces *J. Colloid Interface Sci.* **208** 329–46
[15] Yang J, Lu F, Kostiuk L W and Kwok D Y 2003 Electrokinetic microchannel battery by means of electrokinetic and microfluidic phenomena *J. Micromech. Microeng.* **13** 963–70
[16] Yang C and Li D 1997 Electrokinetic effects on pressure-driven liquid flows in rectangular microchannels *J. Colloid Interface Sci.* **194** 95–107
[17] Vainshtein P and Gutfinger C 2002 On electroviscous effects in microchannels *J. Micromech. Microeng.* **12** 252–6
[18] Chun M-S and Kwak H W 2003 Electrokinetic flow and electroviscous effect in a charged slit-like microfluidic channel with nonlinear Poisson–Boltzmann field *Korea-Australia Rheology J.* **15** 83–90
[19] Rice C L and Whitehead R 1965 Electrokinetic flow in a narrow cylindrical capillary *J. Phys. Chem.* **69** 4017–24
[20] Levine S, Marriott J R, Neale G and Epstein N 1975 Theory of electrokinetic flow in fine cylindrical capillaries at high zeta-potentials *J. Colloid Interface Sci.* **52** 136–49
[21] Yaroshchuk A E, Boiko Y P and Makovetskiy A L 2002 Filtration potential across membranes containing selective layers *Langmuir* **18** 5154–62
[22] Dean J A (ed) 1999 *Lange's Handbook of Chemistry* 15th edn (New York: McGraw-Hill)
[23] Koeneman P B, Busch-Vishniac I J and Wood K L 1997 Feasibility of micro power supplies for MEMS *J. Microelectromech. Syst.* **6** 355–62